

Hadron spectroscopy using the light-front holographic Schrödinger equation and the 't Hooft equation

Mohammad Ahmady^{✉*} and Sugee Lee MacKay[†]

Department of Physics, Mount Allison University, Sackville, New Brunswick, Canada, E4L 1E6

Satvir Kaur[‡]

Department of Physics, Dr. B.R. Ambedkar National Institute of Technology, Jalandhar 144011, India

Chandan Mondal[§]

Institute of Modern Physics, Chinese Academy of Sciences, Lanzhou 730000, China & School of Nuclear Science and Technology, University of Chinese Academy of Sciences, Beijing 100049, China

Ruben Sandapen^{||}

Department of Physics, Acadia University, Wolfville, Nova-Scotia, Canada, B4P 2R6



(Received 10 August 2021; accepted 27 September 2021; published 18 October 2021)

Light-front holographic QCD provides a successful first approximation to hadron spectroscopy in the chiral limit of $(3+1)$ -dim light-front QCD, where a holographic Schrödinger-like equation, with an emerging confining scale, κ , governs confinement in the transverse direction. In its supersymmetric formulation, light-front holography predicts that each baryon has two superpartners: a meson and a tetraquark, with their degenerate masses being generated by the same scale, κ . In nature, this mass degeneracy is lifted by chiral symmetry breaking and longitudinal confinement. In this paper, we show that the latter can be successfully captured by the 't Hooft equation of $(1+1)$ -dim, large N_c , QCD. Together, the holographic Schrödinger equation and the 't Hooft equation provide a good global description of the data across the full hadron spectrum with a universal κ .

DOI: 10.1103/PhysRevD.104.074013

I. INTRODUCTION

In light-front $(3+1)$ -dim QCD, the mass of a quark-antiquark meson is given by [1]

$$M^2 = \int dx d^2\mathbf{b}_\perp \Psi^*(x, \mathbf{b}_\perp) \left[-\frac{\nabla_{b_\perp}^2}{x(1-x)} + \frac{m_q^2}{x} + \frac{m_{\bar{q}}^2}{1-x} \right] \times \Psi(x, \mathbf{b}_\perp) + \text{interactions}, \quad (1)$$

where $\Psi(x, \mathbf{b}_\perp)$ is the meson light-front wave function, x the light-front momentum fraction carried by the quark, and \mathbf{b}_\perp (or $b_\perp e^{i\varphi}$ in polar representation) the transverse

distance between the quark and the antiquark. In Eq. (1), m_q and $m_{\bar{q}}$ are the effective quark and antiquark masses, respectively [1]. The ‘‘interactions’’ contain all the complicated QCD dynamics of a bound state, including the effect of higher Fock sectors on the valence sector.

Introducing the light-front variable,

$$\zeta = \sqrt{x(1-x)}\mathbf{b}_\perp, \quad (2)$$

allows a factorization of the wave function into a transverse mode, $\phi(\zeta)$, and a longitudinal mode, $X(x)$:

$$\Psi(x, \zeta, \varphi) = \frac{\phi(\zeta)}{\sqrt{2\pi\zeta}} e^{iL\varphi} X(x), \quad (3)$$

with $L = |L_z^{\max}|$ being the light-front orbital angular momentum, and $X(x) = \sqrt{x(1-x)}\chi(x)$. Equation (1) then becomes

$$M^2 = M_\perp^2 + M_\parallel^2, \quad (4)$$

where

Published by the American Physical Society under the terms of the [Creative Commons Attribution 4.0 International license](#). Further distribution of this work must maintain attribution to the author(s) and the published article's title, journal citation, and DOI. Funded by SCOAP³.

$$M_{\perp}^2 = \int d^2\zeta \phi^*(\zeta) \left[-\frac{d^2}{d\zeta^2} + \frac{4L^2 - 1}{4\zeta^2} + U_{\perp}(\zeta) \right] \phi(\zeta), \quad (5)$$

and

$$M_{\parallel}^2 = \int dx \chi^*(x) \left[\frac{m_q^2}{x} + \frac{m_{\bar{q}}^2}{1-x} + U_{\parallel}(x) \right] \chi(x), \quad (6)$$

with

$$\int dx |\chi(x)|^2 = \int d^2\zeta |\phi(\zeta)|^2 = 1. \quad (7)$$

Here the QCD bound-state dynamics are encoded in the potentials $U_{\perp}(\zeta)$ and $U_{\parallel}(x)$. Their exact derivation from first principles remains an open question.

Light-front holography [1–4] considers the chiral limit, i.e., massless quarks, and neglects longitudinal confinement, thus implying that $M_{\parallel} = 0$. Remarkably, the form of the transverse confinement potential, $U_{\perp}(\zeta)$, is uniquely fixed by the underlying conformal symmetry and a holographic mapping to anti-deSitter AdS₅, resulting in [1–4]

$$U_{\perp}^{\text{LFH}}(\zeta) = \kappa^4 \zeta^2 + 2\kappa^2(J - 1), \quad (8)$$

where $J = L + S$. In this holographic mapping, the variable ζ maps onto the fifth dimension of AdS₅. Equation (5), which can be rewritten as

$$\left(-\frac{d^2}{d\zeta^2} + \frac{4L^2 - 1}{4\zeta^2} + U_{\perp}^{\text{LFH}}(\zeta) \right) \phi(\zeta) = M_{\perp}^2 \phi(\zeta), \quad (9)$$

maps onto the wave equation for the amplitude of spin- J modes propagating in AdS₅ modified by a quadratic dilaton field. In light-front holography, the longitudinal mode, $X(x)$, is hence not dynamical, i.e., undetermined by Eq. (6). It is instead fixed by the holographic mapping of the electromagnetic (or gravitational) pion form factor in physical spacetime and AdS₅ [5,6], resulting in $\chi(x) = 1$, i.e.,

$$X(x) = \sqrt{x(1-x)}. \quad (10)$$

The supersymmetric formulation of light-front holography [7–11] provides a unified description of baryons and mesons/tetraquarks where each baryon (viewed as a quark-diquark system) possesses two superpartners: a (quark-antiquark) meson and a (diquark-antidiquark) tetraquark. This supersymmetric connection stems from the fact that a diquark can be in the same SU_c(3) representation as an antiquark, and an antidiquark can be in the same SU_c(3) representation as a quark. The supersymmetric holographic Schrödinger equation reads [9]

$$H|\phi\rangle = M_{\perp}^2|\phi\rangle, \quad (11)$$

where

$$H = \begin{pmatrix} -\frac{d^2}{d\zeta^2} + \frac{4L_M^2 - 1}{4\zeta^2} + U_M(\zeta) & 0 \\ 0 & -\frac{d^2}{d\zeta^2} + \frac{4L_B^2 - 1}{4\zeta^2} + U_B(\zeta) \end{pmatrix}, \quad (12)$$

with

$$U_M(\zeta) = \kappa^4 \zeta^2 + 2\kappa^2(L_M + S_M - 1), \quad (13)$$

$$U_B(\zeta) = \kappa^4 \zeta^2 + 2\kappa^2(L_B + S_D), \quad (14)$$

where S_M is the total quark-antiquark spin and S_D is the diquark spin. The 4-plet, $|\phi\rangle$, is given by

$$|\phi\rangle = \begin{pmatrix} \phi_M(L_M = L_B + 1) & \psi^-(L_B + 1) \\ \psi^+(L_B) & \phi_T(L_T = L_B) \end{pmatrix}, \quad (15)$$

where ψ^+ and ψ^- are the two components of the baryon wave function and $\phi_{M/T}$ is the meson/tetraquark wave function. Equation (11) admits analytical solutions, with its eigenvalues given by

$$M_{\perp,M}^2 = 4\kappa^2 \left(n_{\perp} + L_M + \frac{S_M}{2} \right), \quad (16)$$

$$M_{\perp,B}^2 = 4\kappa^2 \left(n_{\perp} + L_B + \frac{S_D}{2} + 1 \right), \quad (17)$$

and

$$M_{\perp,T}^2 = 4\kappa^2 \left(n_{\perp} + L_T + \frac{S_T}{2} + 1 \right), \quad (18)$$

where n_{\perp} is the principal quantum number that emerges when solving the holographic Schrödinger equation, and S_T is total diquark-antidiquark spin.

It follows that baryons with quantum numbers, $L_B = L_M - 1$ and $S_D = S_M$, are superpartners to mesons with quantum numbers, L_M and S_M , and tetraquarks with quantum numbers $S_T = S_D$ and $L_T = L_B$. Hence, within a given family of superpartners, we can write $S \equiv S_D = S_M = S_T$. Note that the lowest-lying mesons with $n_{\perp} = L_M = 0$ do not have a baryonic superpartner. Furthermore, pseudoscalar mesons with $n_{\perp} = L_M = S_M = 0$, like the pion and the kaon, are predicted to be massless, just as expected in the chiral limit of QCD.

II. CHIRAL SYMMETRY BREAKING AND LONGITUDINAL CONFINEMENT

The effects of nonzero quark masses were originally taken into account using a prescription by Brodsky and de Téramond (BdT) [12], which relies on the fact that the holographic ground state wave function depends on the invariant mass of the $q\bar{q}$ pair. Indeed, in momentum space,

$$\tilde{\phi}(x, \mathbf{k}) \propto \frac{1}{\sqrt{x(1-x)}} \exp\left(-\frac{M_{q\bar{q}}^2}{2\kappa^2}\right), \quad (19)$$

where

$$M_{q\bar{q}}^2 = \frac{\mathbf{k}^2}{x(1-x)} \quad (20)$$

is the invariant mass of the $q\bar{q}$ pair, with \mathbf{k} being the transverse momentum of the quark. For massive quarks, the invariant mass becomes

$$M_{q\bar{q}}^2 = \frac{\mathbf{k}^2}{x(1-x)} + \frac{m_q^2}{x} + \frac{m_{\bar{q}}^2}{1-x}. \quad (21)$$

Thus, after Fourier transforming back to position space, the BdT prescription amounts to a modification of the longitudinal mode:

$$X_{\text{BdT}}(x) = \sqrt{x(1-x)} \chi_{\text{BdT}}(x), \quad (22)$$

where

$$\chi_{\text{BdT}}(x) = \exp\left(-\frac{(1-x)m_q^2 + xm_{\bar{q}}^2}{2\kappa^2 x(1-x)}\right). \quad (23)$$

Treating the kinetic energy of massive quarks as a first-order perturbation to the holographic potential, Eq. (8), the resulting first-order shift to $M = M_\perp$ due to quark masses is then given by

$$\Delta M_{\text{BdT}}^2 = \int dx \chi_{\text{BdT}}^2(x) \left(\frac{m_q^2}{x} + \frac{m_{\bar{q}}^2}{1-x}\right), \quad (24)$$

so that the pion mass $M_\pi = \Delta M_{\text{BdT}}$. Similarly, the kaon mass $M_K = \Delta M_{\text{BdT}}$ when the strange quark is taken into account. Equation (24) can be generalized for baryons and tetraquarks [11]:

$$\Delta M_{\text{BdT}}^2 = \frac{\lambda^2}{F} \frac{dF[\lambda]}{d\lambda}, \quad (25)$$

where

$$F[\lambda] = \int_0^1 \prod_{i=1}^n dx_i e^{-\frac{1}{\lambda} \sum_j^n m_j^2/x_j} \delta\left(\sum_j x_j - 1\right), \quad (26)$$

with $\lambda = \kappa^2$. Note that Eq. (25) coincides with Eq. (24) for $n = 2$.

Strictly speaking, Eq. (24) is only accurate for light hadrons in their ground states. However, as a first approximation, it is not unreasonable to assume the same correction for excited states. At the same time, this guarantees that the predicted Regge trajectories remain linear. Indeed, Eq. (24), together with Eqs. (16), (17), and (18), have been used to fit the light hadron spectrum in Ref. [11], resulting in a universal $\kappa = 0.523 \pm 0.024$ GeV, with $m_{u/d} = 0.046$ GeV and $m_s = 0.357$ GeV. The use of Eq. (24) has also been extrapolated to heavy quarks in order to predict the heavy-light and heavy-heavy hadron spectra in Refs. [7,8,10], with the requirement that κ is no longer universal in the heavy hadron sector. In an attempt to protect the universality of κ in the heavy sector, Ref. [13] introduces another mass scale (instead of κ) in Eq. (23).

A theoretical shortcoming of Eq. (24) is that, in the chiral limit, it predicts [14] $M_\pi^2 \propto 2m_{u/d}^2(\ln \kappa^2/m_{u/d}^2 - \gamma_E)$, where $\gamma_E \approx 0.577216$ is Euler's constant, which is not consistent with the Gell-Mann-Oakes-Renner (GMOR) relation [15], which states that $M_\pi^2 \propto m_{u/d}$ in the chiral limit. An improved ansatz, consistent with the GMOR relation, has been proposed in Ref. [16]. Recently, this shortcoming has been more rigorously addressed in Refs. [14,17] by solving Eq. (6) with a longitudinal confining potential [18,19]

$$U_{\parallel}(x) = -\sigma^2 \partial_x(x(1-x)) \partial_x, \quad (27)$$

where σ is a mass scale. Reference [14] studies light mesons including their excited states while Ref. [17] focuses on the ground states of light and heavy mesons. While using Eq. (27), Ref. [17] also discusses the relation of their approach to the 't Hooft equation. The idea to use the 't Hooft equation to go beyond the BdT prescription was first proposed in Ref. [20], with the unique goal of predicting the meson decay constants while leaving the predicted mass spectrum unchanged. The latter constraint is imposed by subtracting M_{\parallel}^2 from the 't Hooft potential.

In this paper, we use the 't Hooft equation (without shifting the 't Hooft potential as in Ref. [20]), together with the holographic Schrödinger equation, to compute the full hadron spectrum, i.e., the masses of the ground and excited states of mesons, baryons, and tetraquarks, including those with one or two heavy quarks. In Ref. [21], only the meson spectrum was studied. We shall also compare our results with the mass spectrum obtained using the alternative longitudinal potential given by Eq. (27).

TABLE I. Quark masses and longitudinal confinement scale, g , in GeV used in conjunction with the 't Hooft potential. Note that we use $\kappa = 0.523$ GeV for all hadrons, and that it coincides with g for hadrons with two heavy quarks.

Hadron	g	$m_{u/d}$	m_s	m_c	m_b
Light	0.128	0.046	0.357
Heavy-light	0.410	0.330	0.500	1.370	4.640
Heavy-heavy	0.523	1.370	4.640

III. THE 'T HOOFT EQUATION

The 't Hooft equation is derived from the QCD Lagrangian in $(1+1)$ -dim and in the large $-N_c$ approximation where only planar diagrams contribute. The result is [22]

$$\left(\frac{m_q^2}{x} + \frac{m_{\bar{q}}^2}{1-x}\right)\chi(x) + \frac{g^2}{\pi} \mathcal{P} \int dy \frac{|\chi(x) - \chi(y)|}{(x-y)^2} = M_{||}^2 \chi(x), \quad (28)$$

where $g = g_s \sqrt{N_c}$ is the (finite) 't Hooft coupling and \mathcal{P} denotes the principal value prescription. Note that Eq. (28) can also be derived in the continuum limit of discretized

$(1+1)$ -dim light-front QCD [23]. We use the 't Hooft equation for baryons and tetraquarks by making the transformation $\bar{q} \rightarrow [qq]$ for baryons, followed by $q \rightarrow [\bar{q}\bar{q}]$ for tetraquarks. Since the color interaction is invariant under these transformations, the longitudinal confinement scale, g , remains the same within a family of superpartners. The 't Hooft equation has been extensively studied in the literature [24–32] and it is worth noting that, in the conformal limit, it possesses a gravity dual on AdS_3 [33]. Here, we only highlight how it is both complementary and consistent with the holographic Schrödinger equation

First, assuming a 't Hooft wave function of the form [17]

$$\chi(x) \approx x^{\beta_1} (1-x)^{\beta_2}, \quad (29)$$

then, near the endpoints, $x \rightarrow 0, 1$,

$$\frac{\pi m_i^2}{g^2} - 1 + \pi \beta_i \cot(\pi \beta_i) = 0. \quad (30)$$

Eq. (30) implies that, in the chiral limit, $m_i \rightarrow 0$,

$$\beta_i = \sqrt{3m_i^2/\pi g^2} \quad (31)$$

and

TABLE II. Computed masses (in MeV), using the 't Hooft potential, for the light hadrons compared to the PDG data [36].

Meson				Baryon						Tetraquark				
$J^{P(C)}$	Name	$M_{ }$	M_{\perp}	M	$J^{P(C)}$	Name	$M_{ }$	M_{\perp}	M	$J^{P(C)}$	Name	$M_{ }$	M_{\perp}	M
0 ⁺	$\pi(140)$	140	0	140
1 ⁺⁻	$h_1(1170)$	335	1046	1098	(1/2) ⁺	$N(940)$	188	1046	1063	0 ⁺⁺	$f_0(500)$	335	1046	1098
2 ⁺⁻	$\eta_2(1645)$	460	1479	1549	(3/2) ⁻	$N(1520)$	296	1479	1508	1 ⁺⁺	...	408	1479	1534
1 ⁻⁻	$\rho(770), \omega(780)$	140	740	753
2 ⁺⁺	$a_2(1320), f_2(1270)$	335	1281	1324	(3/2) ⁺	$\Delta(1232)$	188	1281	1295	1 ⁺⁺	$a_1(1260)$	235	1281	1302
3 ⁻⁻	$\rho_3(1690), \omega_3(1670)$	460	1654	1717	(3/2) ⁻	$\Delta(1700)$	296	1654	1680	1 ⁺⁺	$\pi_1(1600)$	335	1654	1688
4 ⁺⁺	$a_4(1970), f_4(2050)$	559	1957	2035	(7/2) ⁺	$\Delta(1950)$	372	1957	1992
0 ⁻	$\bar{K}(495)$	456	0	456
1 ⁺	$\bar{K}_1(1270)$	550	1046	1182	(1/2) ⁺	$\Lambda(1115)$	500	1046	1159	0 ⁺	$K_0^*(1430)$	546	1046	1180
2 ⁻	$K_2(1770)$	617	1479	1603	(3/2) ⁻	$\Lambda(1520)$	588	1479	1592	1 ⁻	...	633	1479	1609
0 ⁻	$\bar{K}(495)$	456	0	456
1 ⁺	$\bar{K}_1(1270)$	550	1046	1182	(1/2) ⁺	$\Sigma(1190)$	500	1046	1159	0 ⁺⁺	$a_0(980)$	920	1046	1393
											$f_0(980)$			
1 ⁻	$K^*(890)$	456	740	869
2 ⁺	$K_2^*(1430)$	550	1281	1394	(3/2) ⁺	$\Sigma(1385)$	500	1281	1375	1 ⁺	$K_1(1400)$	546	1281	1392
3 ⁻	$K_3^*(1780)$	617	1654	1765	(3/2) ⁻	$\Sigma(1670)$	588	1654	1755	2 ⁻	$K_2(1820)$	633	1654	1771
4 ⁺	$K_4^*(2045)$	672	1957	2069	(7/2) ⁺	$\Sigma(2030)$	650	1957	2062
0 ⁺⁻	$\eta'(958)$	759	0	759
1 ⁺⁻	$h_1(1380)$	883	1046	1369	(1/2) ⁺	$\Xi(1320)$	805	1046	1320	0 ⁺⁺	$f_0(1370)$	920	1046	1393
											$a_0(1450)$			
2 ⁺⁻	$\eta_2(1870)$	968	1479	1768	(3/2) ⁻	$\Xi(1620)$	876	1479	1719	1 ⁺⁺	...	969	1479	1768
1 ⁻⁻	$\Phi(1020)$	759	740	1060
2 ⁺⁺	$f'_2(1525)$	883	1281	1556	(3/2) ⁺	$\Xi^*(1530)$	805	1281	1513	1 ⁺⁺	$f_1(1420)$	850	1281	1537
											$a_1(1420)$			
3 ⁻⁻	$\Phi_3(1850)$	968	1654	1916	(3/2) ⁻	$\Xi(1820)$	876	1654	1872
2 ⁺⁺	$f_2(1640)$	883	1281	1556	(3/2) ⁺	$\Omega(1672)$	1114	1281	1698	1 ⁺	$K_1(1650)$	1159	1281	1728

TABLE III. Computed masses (in MeV), using the 't Hooft potential, for hadrons with one heavy quark, compared to the PDG data [36].

Meson				Baryon						Tetraquark					
$J^{P(C)}$	Name	M_{\parallel}	M_{\perp}	M	$J^{P(C)}$	Name	M_{\parallel}	M_{\perp}	M	$J^{P(C)}$	Name	M_{\parallel}	M_{\perp}	M	
0 ⁻	$D(1870)$	1861	0	1861
1 ⁺	$D_1(2420)$	2135	1046	2377	(1/2) ⁺	$\Lambda_c(2290)$	2191	1046	2428	0 ⁺	$D_0^*(2400)$	2510	1046	2719	
2 ⁻	$D_J(2600)$	2326	1479	2756	(3/2) ⁻	$\Lambda_c(2625)$	2460	1479	2870	1 ⁻	...	2751	1479	3123	
0 ⁻	$\bar{D}(1870)$	1861	0	1861	
1 ⁺	$\bar{D}_1(2420)$	2135	1046	2377	(1/2) ⁺	$\Sigma_c(2455)$	2191	1046	2428	0 ⁺	$D_0^*(2400)$	2510	1046	2719	
1 ⁻	$D^*(2010)$	1861	740	2003	
2 ⁺	$D_2^*(2460)$	2135	1281	2490	(3/2) ⁺	$\Sigma_c^*(2520)$	2191	1281	2538	1 ⁺	$D(2550)$	2510	1281	2818	
3 ⁻	$D_3^*(2750)$	2326	1654	2854	(3/2) ⁻	$\Sigma_c(2800)$	2460	1654	2964	
0 ⁻	$D_s(1968)$	2025	0	2025	
1 ⁺	$D_{s1}(2460)$	2283	1046	2511	(1/2) ⁺	$\Xi_c(2470)$	2348	1046	2570	0 ⁺	$\bar{D}_{s0}^*(2317)$	2676	1046	2873	
2 ⁻	$D_{s2}?$	2464	1479	2874	(3/2) ⁻	$\Xi_c(2815)$	2586	1479	2979	1 ⁻	...	2908	1479	3262	
1 ⁻	$D_s^*(2110)$	2025	740	2156	
2 ⁺	$D_{s2}^*(2573)$	2283	1281	2618	(3/2) ⁺	$\Xi_c^*(2645)$	2348	1281	2675	1 ⁺	$D_{s1}(2536)$	2676	1281	2967	
3 ⁻	$D_{s3}^*(2860)$	2464	1654	2968	
1 ⁺	$\bar{D}_{s1}?$	2283	1046	2511	(1/2) ⁺	$\Omega_c(2695)$	2524	1046	2732	0 ⁺	...	2845	1046	3031	
2 ⁺	$D_{s2}^*?$	2283	1281	2618	(3/2) ⁺	$\Omega_c(2770)$	2524	1281	2830	1 ⁺	...	3012	1281	3273	
0 ⁻	$\bar{B}(5280)$	5130	0	5130	
1 ⁺	$\bar{B}_1(5720)$	5385	1046	5486	(1/2) ⁺	$\Lambda_b(5620)$	5460	1046	5559	0 ⁺	$B_J(5732)$	5775	1046	5869	
2 ⁻	$\bar{B}_J(5970)$	5560	1479	5753	(3/2) ⁻	$\Lambda_b(5920)$	5714	1479	5902	1 ⁻	...	5999	1479	6179	
0 ⁻	$B(5280)$	5130	0	5130	
1 ⁺	$B_1(5720)$	5385	1046	5486	(1/2) ⁺	$\Sigma_b(5815)$	5460	1046	5559	0 ⁺	$\bar{B}_J(5732)$	5775	1046	5869	
1 ⁻	$B^*(5325)$	5130	740	5183	
2 ⁺	$B_2^*(5747)$	5385	1281	5535	(3/2) ⁺	$\Sigma_b^*(5835)$	5460	1281	5608	1 ⁺	$B_J(5840)$	5775	1281	5915	
0 ⁻	$B_s(5365)$	5292	0	5292	
1 ⁺	$B_{s1}(5830)$	5528	1046	5626	(1/2) ⁺	$\Xi_b(5790)$	5610	1046	5707	0 ⁺	$\bar{B}_{s0}^*?$	5936	1046	6027	
1 ⁻	$B_s^*(5415)$	5292	740	5343	
2 ⁺	$B_{s2}^*(5840)$	5528	1281	5674	(3/2) ⁺	$\Xi_b^*(5950)$	5610	1281	5754	1 ⁺	$B_{s1}?$	5936	1281	6073	
1 ⁺	$B_{s1}?$	5528	1046	5626	(1/2) ⁺	$\Omega_b(6045)$	5791	1046	5885	0 ⁺	...	6110	1046	6199	

TABLE IV. Computed masses (in MeV), using the 't Hooft potential, for hadrons with two heavy quarks, compared to the PDG data [36].

Meson				Baryon						Tetraquark					
$J^{P(C)}$	Name	M_{\parallel}	M_{\perp}	M	$J^{P(C)}$	Name	M_{\parallel}	M_{\perp}	M	$J^{P(C)}$	Name	M_{\parallel}	M_{\perp}	M	
0 ⁺	$\eta_c(2984)$	2927	0	2927
1 ⁺⁻	$h_c(3525)$	3440	1046	3596	(1/2) ⁺	$\Xi_{cc}^{\text{SELEX}}(3520)$ $\Xi_{cc}^{\text{LHCb}}(3620)$	3254	1046	3418	0 ⁺⁺	$\chi_{c0}(3415)$	3864	1046	4003	
1 ⁻⁻	$J/\psi(3096)$	2927	740	3019
2 ⁺⁺	$\chi_{c2}(3556)$	3440	1281	3671	(3/2) ⁺	$\Xi_{cc}^{\text{LHCb}}(3620)$	3254	1281	3497	1 ⁺⁺	$\chi_{c1}(3510)$	3580	1281	3802	
1 ⁻⁻	$\psi'(3686)$	3440	1281	3671	
2 ⁺⁺	$\chi_{c2}(3927)$	3794	1654	4139	(3/2) ⁺	$\Xi_{cc}^?$	3751	1654	4099	1 ⁺⁺	$X(3872)$	4062	1654	4386	
										1 ⁺⁻	$Z_c(3900)$	4240	1654	4551	
0 ⁺	$\eta_b(9400)$	9424	0	9424
1 ⁺⁻	$h_b(9900)$	9776	1046	9832	(1/2) ⁺	$\Xi_{bb}?$	9750	1046	9806	0 ⁺⁺	$\chi_{b0}(9860)$	10285	1046	10338	
1 ⁻⁻	$\Upsilon(9460)$	9424	740	9453	
2 ⁺⁺	$\chi_{b2}(9910)$	9776	1281	9860	(3/2) ⁺	$\Xi_{bb}?$	9750	1281	9834	1 ⁺⁺	$\chi_{b1}(9893)$	10081	1281	10162	
1 ⁻⁻	$\Upsilon(2S)(10020)$	9776	1281	9860	
2 ⁺⁺	$\chi_{b2}(10270)$	10024	1654	10160	(3/2) ⁺	$\Xi_{bb}?$	10100	1654	10234	1 ⁺⁺	$X_b?$	10425	1654	10555	

TABLE V. Computed masses (in MeV) using the alternative longitudinal potential given by Eq. (27), for light hadrons compared to the PDG data [36].

Meson			Baryon						Tetraquark					
$J^{P(C)}$	Name	M_{\parallel}	M_{\perp}	M	$J^{P(C)}$	Name	M_{\parallel}	M_{\perp}	M	$J^{P(C)}$	Name	M_{\parallel}	M_{\perp}	M
0^{-+}	$\pi(140)$	140	0	140	\dots	\dots	\dots	\dots	\dots	\dots	\dots	\dots	\dots	\dots
1^{+-}	$h_1(1170)$	387	1046	1115	$(1/2)^+$	$N(940)$	189	1046	1063	0^{++}	$f_0(500)$	359	1046	1106
2^{-+}	$\eta_2(1645)$	629	1479	1607	$(3/2)^-$	$N(1520)$	312	1479	1512	1^{+-}	\dots	480	1479	1555
1^{--}	$\rho(770), \omega(780)$	140	740	753	\dots	\dots	\dots	\dots	\dots	\dots	\dots	\dots	\dots	\dots
2^{++}	$a_2(1320), f_2(1270)$	387	1281	1338	$(3/2)^+$	$\Delta(1232)$	189	1281	1295	1^{++}	$a_1(1260)$	236	1281	1302
3^{--}	$\rho_3(1690), \omega_3(1670)$	629	1654	1770	$(3/2)^-$	$\Delta(1700)$	312	1654	1683	1^{+-}	$\pi_1(1600)$	359	1654	1692
4^{++}	$a_4(1970), f_4(2050)$	870	1957	2142	$(7/2)^+$	$\Delta(1950)$	434	1957	2004	\dots	\dots	\dots	\dots	\dots
0^-	$\bar{K}(495)$	459	0	459	\dots	\dots	\dots	\dots	\dots	\dots	\dots	\dots	\dots	\dots
1^+	$\bar{K}_1(1270)$	580	1046	1196	$(1/2)^+$	$\Lambda(1115)$	505	1046	1162	0^+	$K_0^*(1430)$	552	1046	1183
2^-	$K_2(1770)$	700	1479	1636	$(3/2)^-$	$\Lambda(1520)$	626	1479	1606	1^-	\dots	672	1479	1624
0^-	$\bar{K}(495)$	459	0	459	\dots	\dots	\dots	\dots	\dots	\dots	\dots	\dots	\dots	\dots
1^+	$\bar{K}_1(1270)$	580	1046	1196	$(1/2)^+$	$\Sigma(1190)$	505	1046	1162	0^{++}	$a_0(980)$	984	1046	1436
\dots	\dots	\dots	\dots	\dots	\dots	\dots	\dots	\dots	\dots	\dots	$f_0(980)$	\dots	\dots	\dots
1^-	$K^*(890)$	459	740	871	\dots	\dots	\dots	\dots	\dots	\dots	\dots	\dots	\dots	\dots
2^+	$K_2^*(1430)$	580	1281	1406	$(3/2)^+$	$\Sigma(1385)$	505	1281	1377	1^+	$K_1(1400)$	552	1281	1395
3^-	$K_3^*(1780)$	700	1654	1796	$(3/2)^-$	$\Sigma(1670)$	626	1654	1768	2^-	$K_2(1820)$	672	1654	1785
4^+	$K_4^*(2045)$	821	1957	2122	$(7/2)^+$	$\Sigma(2030)$	747	1957	2095	\dots	\dots	\dots	\dots	\dots
0^{-+}	$\eta'(958)$	772	0	772	\dots	\dots	\dots	\dots	\dots	\dots	\dots	\dots	\dots	\dots
1^{+-}	$h_1(1380)$	1012	1046	1455	$(1/2)^+$	$\Xi(1320)$	818	1046	1328	0^{++}	$f_0(1370)$	984	1046	1436
\dots	\dots	\dots	\dots	\dots	\dots	\dots	\dots	\dots	\dots	\dots	$a_0(1450)$	\dots	\dots	\dots
2^{+-}	$\eta_2(1870)$	1252	1479	1938	$(3/2)^-$	$\Xi(1620)$	938	1479	1751	1^{+-}	\dots	1104	1479	1846
1^{--}	$\Phi(1020)$	772	740	1069	\dots	\dots	\dots	\dots	\dots	\dots	\dots	\dots	\dots	\dots
2^{++}	$f'_2(1525)$	1012	1281	1632	$(3/2)^+$	$\Xi^*(1530)$	818	1281	1520	1^{++}	$f_1(1420)$	864	1281	1545
\dots	\dots	\dots	\dots	\dots	\dots	\dots	\dots	\dots	\dots	\dots	$a_1(1420)$	\dots	\dots	\dots
3^{--}	$\Phi_3(1850)$	1252	1654	2074	$(3/2)^-$	$\Xi(1820)$	938	1654	1901	\dots	\dots	\dots	\dots	\dots
2^{++}	$f_2(1640)$	1012	1281	1632	$(3/2)^+$	$\Omega(1672)$	1129	1281	1708	1^+	$K_1(1650)$	1175	1281	1738

$$M_\pi^2 = g \sqrt{\frac{\pi}{3}} (m_u + m_d) + \mathcal{O}(m_u + m_d)^2. \quad (32)$$

Since, via Eq. (16), the holographic Schrödinger Equation predicts a massless pion, it follows that the only contribution to the pion mass is generated by the 't Hooft Equation. Thus, together, the holographic Schrödinger Equation and the 't Hooft Equation correctly predicts the GMOR relation, $M_\pi^2 \sim m_{u/d}$. Notice also that in the chiral limit, $\beta_i \rightarrow 0$ and $\chi(x) = 1$ as in light-front holography.

Second, as already noted in Ref. [21], the 't Hooft potential is consistent with the holographic potential in that they both correspond to a linear confining potential in the non-relativistic limit, with $g = \kappa$ [21]. To show this, first note that the 't Hooft potential in position space reads

$$U_{\parallel}^{\text{tHooft}}(x^-) = \frac{g^2}{2} P^+ |x^-| = g^2 P^+ b_{\parallel}, \quad (33)$$

where $x^- = x^0 - x^3$ is the light-front longitudinal distance, and P^+ is the light-front longitudinal momentum of the meson. The second equality follows from the fact that $x^+ = x^0 + x^3 = 0$, so that $|x^-| = 2|x^3| \equiv 2b_{\parallel}$. Note that

$\tilde{z} = P^+ x^-$ is the frame-independent longitudinal coordinate of Ref. [34].

Using the general relation between a frame-invariant light-front (LF) potential and a center of mass (CM) frame instant-form (IF) potential [35]:

$$U_{\text{LF}} = V_{\text{IF}}^2 + 4mV_{\text{IF}}, \quad (34)$$

it follows from Eq. (34) that the (chiral-limit) quadratic light-front holographic potential, Eq. (8), corresponds to a linear instant form potential. The light-front 't Hooft potential, Eq. (33), also corresponds to a linear instant form potential in the heavy quark (non-relativistic) limit where $m_Q \gg g$ and $P^+ \rightarrow 2m_Q$, where m_Q is the heavy quark mass. In this non-relativistic limit, it is also appropriate to take $x \rightarrow 1/2$ in Eq. (8). Therefore, we see that, in the non-relativistic limit, the holographic potential and the 't Hooft potential are both equivalent to CM-frame linear instant-form potentials:

$$V_{\perp} \rightarrow \frac{1}{2} \kappa^2 b_{\perp}, \quad (35)$$

and

TABLE VI. Computed masses (in MeV), using the alternative longitudinal potential given by Eq. (27), for hadrons with one heavy quark, compared to the PDG data [36].

Meson					Baryon					Tetraquark				
$J^{P(C)}$	Name	M_{\parallel}	M_{\perp}	M	$J^{P(C)}$	Name	M_{\parallel}	M_{\perp}	M	$J^{P(C)}$	Name	M_{\parallel}	M_{\perp}	M
0 ⁻	$D(1870)$	1859	0	1859
1 ⁺	$D_1(2420)$	1979	1160	2294	(1/2) ⁺	$\Lambda_c(2290)$	2189	1160	2478	0 ⁺	$\bar{D}_0^*(2400)$	2519	1160	2774
2 ⁻	$D_J(2600)$	2099	1640	2664	(3/2) ⁻	$\Lambda_c(2625)$	2309	1640	2833	1 ⁻	...	2639	1640	3108
0 ⁻	$\bar{D}(1870)$	1859	0	1859
1 ⁺	$\bar{D}_1(2420)$	1979	1160	2294	(1/2) ⁺	$\Sigma_c(2455)$	2189	1160	2478	0 ⁺	$D_0^*(2400)$	2519	1160	2774
1 ⁻	$D^*(2010)$	1859	820	2032
2 ⁺	$D_2^*(2460)$	1979	1421	2436	(3/2) ⁺	$\Sigma_c^*(2520)$	2189	1421	2610	1 ⁺	$D(2550)$	2519	1421	2892
3 ⁻	$D_3^*(2750)$	2099	1834	2788	(3/2) ⁻	$\Sigma_c(2800)$	2309	1834	2949
0 ⁻	$D_s(1968)$	2029	0	2029
1 ⁺	$D_{s1}(2460)$	2149	1160	2442	(1/2) ⁺	$\Xi_c(2470)$	2359	1160	2629	0 ⁺	$\bar{D}_{s0}^*(2317)$	2689	1160	2929
2 ⁻	$D_{s2}?$	2269	1640	2800	(3/2) ⁻	$\Xi_c(2815)$	2479	1640	2973	1 ⁻	...	2809	1640	3253
1 ⁻	$D_s^*(2110)$	2029	820	2189
2 ⁺	$D_{s2}^*(2573)$	2149	1421	2576	(3/2) ⁺	$\Xi_c^*(2645)$	2359	1421	2754	1 ⁺	$D_{s1}(2536)$	2689	1421	3042
3 ⁻	$D_{s3}^*(2860)$	2269	1834	2918
1 ⁺	$\bar{D}_{s1}?$	2149	1160	2442	(1/2) ⁺	$\Omega_c(2695)$	2529	1160	2783	0 ⁺	...	2859	1160	3086
2 ⁺	$D_{s2}^*?$	2149	1421	2576	(3/2) ⁺	$\Omega_c(2770)$	2529	1421	2901	1 ⁺	...	2859	1421	3193
0 ⁻	$\bar{B}(5280)$	5060	0	5060
1 ⁺	$\bar{B}_1(5720)$	5180	2000	5552	(1/2) ⁺	$\Lambda_b(5620)$	5390	2000	5749	0 ⁺	$B_J(5732)$	5720	2000	6059
2 ⁻	$\bar{B}_J(5970)$	5300	2828	6007	(3/2) ⁻	$\Lambda_b(5920)$	5510	2828	6193	1 ⁻	...	5840	2828	6489
0 ⁻	$B(5280)$	5060	0	5060
1 ⁺	$B_1(5720)$	5180	2000	5552	(1/2) ⁺	$\Sigma_b(5815)$	5390	2000	5749	0 ⁺	$\bar{B}_J(5732)$	5720	2000	6059
1 ⁻	$B^*(5325)$	5060	1414	5254
2 ⁺	$B_2^*(5747)$	5180	2449	5730	(3/2) ⁺	$\Sigma_b^*(5835)$	5390	2449	5920	1 ⁺	$B_J(5840)$	5720	2449	6222
0 ⁻	$B_s(5365)$	5230	0	5230
1 ⁺	$B_{s1}(5830)$	5350	2000	5711	(1/2) ⁺	$\Xi_b(5790)$	5597	2000	5908	0 ⁺	$\bar{B}_{s0}^*?$	5890	2000	6220
1 ⁻	$B_s^*(5415)$	5230	1414	5418
2 ⁺	$B_{s2}^*(5840)$	5350	2449	5884	(3/2) ⁺	$\Xi_b^*(5950)$	5560	2449	6075	1 ⁺	$B_{s1}?$	5890	2449	6379
1 ⁺	$B_{s1}?$	5350	2000	5711	(1/2) ⁺	$\Omega_b(6045)$	5730	2000	6069	0 ⁺	...	6060	2000	6381

TABLE VII. Computed masses (in MeV), using the alternative longitudinal potential given by Eq. (27), for hadrons with two heavy quarks, compared to the PDG data [36].

Meson					Baryon					Tetraquark				
$J^{P(C)}$	Name	M_{\parallel}	M_{\perp}	M	$J^{P(C)}$	Name	M_{\parallel}	M_{\perp}	M	$J^{P(C)}$	Name	M_{\parallel}	M_{\perp}	M
0 ⁺	$\eta_c(2984)$	2999	0	2999
1 ⁺⁻	$h_c(3525)$	3239	1200	3454	(1/2) ⁺	$\Xi_{cc}^{\text{SELEX}}(3520)$ $\Xi_{cc}^{\text{LHCb}}(3620)$	3329	1200	3539	0 ⁺⁺	$\chi_{c0}(3415)$	3780	1200	3965
1 ⁻⁻	$J/\psi(3096)$	2999	848	3117
2 ⁺⁺	$\chi_{c2}(3556)$	3239	1470	3557	(3/2) ⁺	$\Xi_{cc}^{\text{LHCb}}(3620)$	3329	1470	3639	1 ⁺⁺	$\chi_{c1}(3510)$	3660	1470	3944
1 ⁻⁻	$\psi'(3686)$	3239	1470	3557
2 ⁺⁺	$\chi_{c2}(3927)$	3479	1897	3963	(3/2) ⁺	Ξ_{cc}^* ?	3570	1897	4042	1 ⁺⁺	$X(3872)$	3900	1897	4337
										1 ⁺⁻	$Z_c(3900)$	4020	1897	4445
0 ⁺	$\eta_b(9400)$	9400	0	9400
1 ⁺⁻	$h_b(9900)$	9640	2140	9874	(1/2) ⁺	$\Xi_{bb}?$	9730	2140	9962	0 ⁺⁺	$\chi_{b0}(9860)$	10180	2140	10402
1 ⁻⁻	$\Upsilon(9460)$	9400	1513	9521
2 ⁺⁺	$\chi_{b2}(9910)$	9640	2621	9990	(3/2) ⁺	$\Xi_{bb}?$	9730	2621	10077	1 ⁺⁺	$\chi_{b1}(9893)$	10060	2621	10396
1 ⁻⁻	$\Upsilon(2S)(10020)$	9640	1513	9990
2 ⁺⁺	$\chi_{b2}(10270)$	9880	3384	10443	(3/2) ⁺	$\Xi_{bb}?$	9970	3384	10528	1 ⁺⁺	$X_b?$	10300	3384	10841

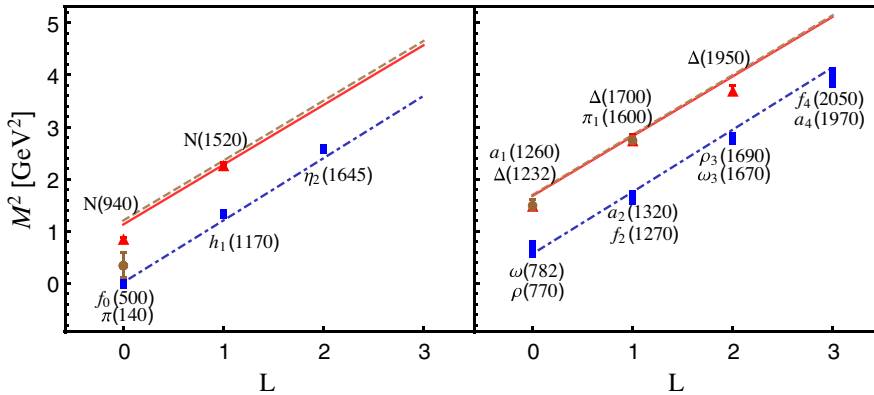


FIG. 1. Regge trajectories for the supersymmetric meson-baryon-tetraquark partners for the unflavored light-light sector. The results are compared to the PDG data [36]. The mesons, baryons, and tetraquarks trajectories are the dot-dashed blue, solid-red, and dashed-brown lines, respectively. For the left panels, $S = 0$ and for the right panels, $S = 1$.

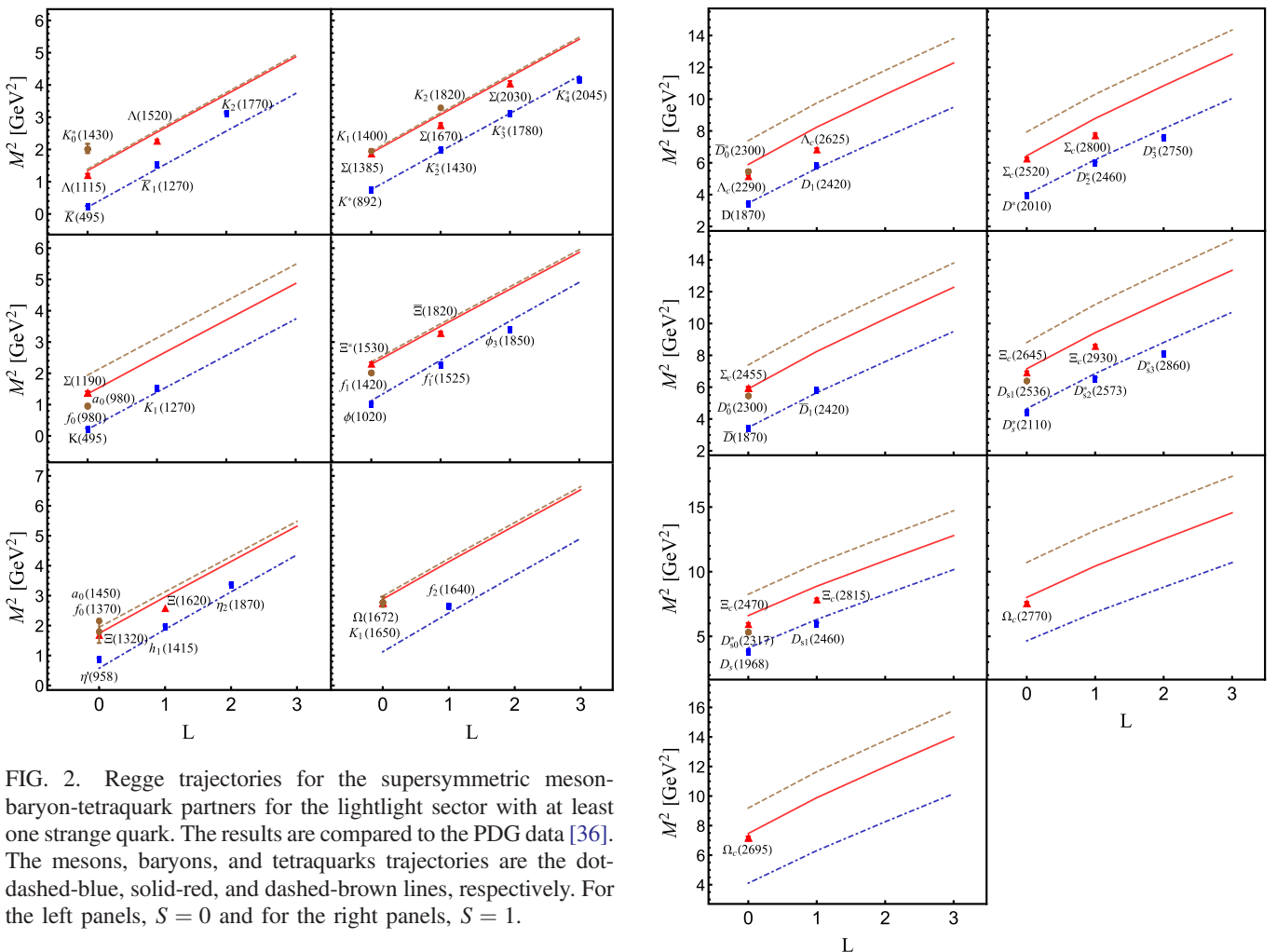


FIG. 2. Regge trajectories for the supersymmetric meson-baryon-tetraquark partners for the light-light sector with at least one strange quark. The results are compared to the PDG data [36]. The mesons, baryons, and tetraquarks trajectories are the dot-dashed-blue, solid-red, and dashed-brown lines, respectively. For the left panels, $S = 0$ and for the right panels, $S = 1$.

$$V_{\parallel} \rightarrow \frac{1}{2} g^2 b_{\parallel}. \quad (36)$$

It then follows that $V_{\perp} = V_{\parallel}$, i.e., rotational symmetry is restored in the CM frame of a heavy-heavy meson if $g = \kappa$.

FIG. 3. Regge trajectories for the supersymmetric meson-baryon-tetraquark partners for the heavy-light sector with one charm quark. The results are compared to the PDG data [36]. The mesons, baryons, and tetraquarks trajectories are indicated by dot-dashed-blue, solid-red, and dashed-brown lines, respectively. For the left panels, $S = 0$ and for the right panels, $S = 1$.

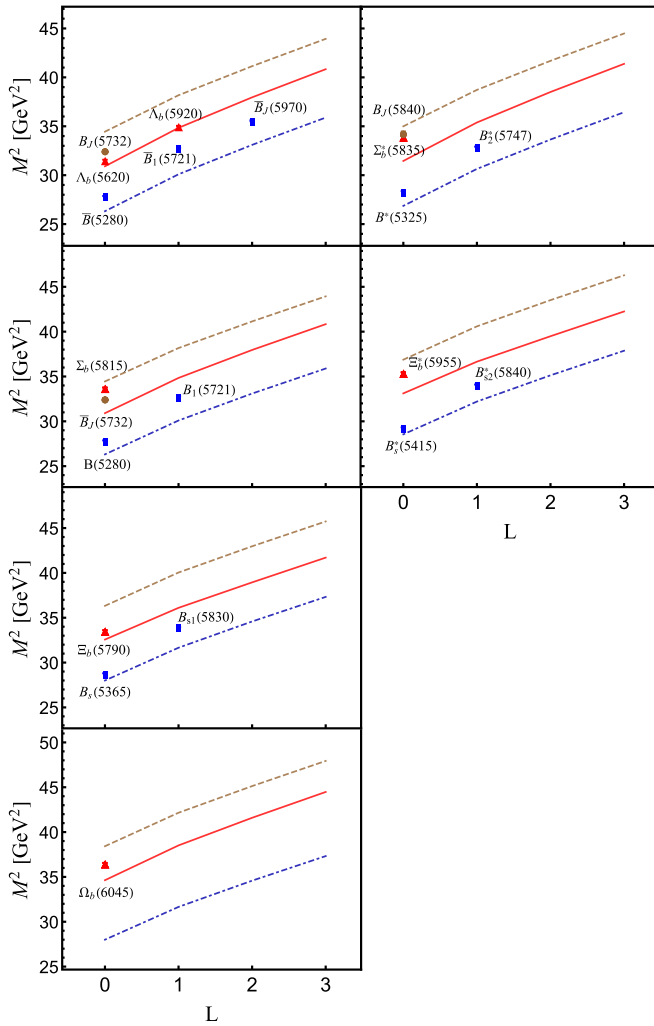


FIG. 4. Regge trajectories for the supersymmetric meson-baryon-tetraquark partners for the heavy-light sector with one bottom quark. The results are compared to the PDG data [36]. The mesons, baryons, and tetraquarks trajectories are indicated by dot-dashed-blue, solid-red, and dashed-brown lines, respectively. For the left panels, $S = 0$ and for the right panels, $S = 1$.

Third, when solving the 't Hooft Equation, an additional quantum number, which we shall label as n_{\parallel} , emerges. Thus, each hadronic state is identified by four quantum numbers, $n_{\perp}, L, S, n_{\parallel}$, with their squared masses given by

$$M_M^2 = M_{\perp,M}^2(n_{\perp}, L_M, S_M, \kappa) + M_{\parallel,M}^2(n_{\parallel}, m_q, m_{\bar{q}}, g), \quad (37)$$

$$M_B^2 = M_{\perp,B}^2(n_{\perp}, L_B, S_D, \kappa) + M_{\parallel,B}^2(n_{\parallel}, m_q, m_{[qq]}, g), \quad (38)$$

$$M_T^2 = M_{\perp,T}^2(n_{\perp}, L_T, S_T, \kappa) + M_{\parallel,T}^2(n_{\parallel}, m_{[\bar{q}\bar{q}]}, m_{[qq]}, g), \quad (39)$$

and their parity given by

$$P = (-1)^{L_M+1} = (-1)^{L_B} = (-1)^{L_T}. \quad (40)$$

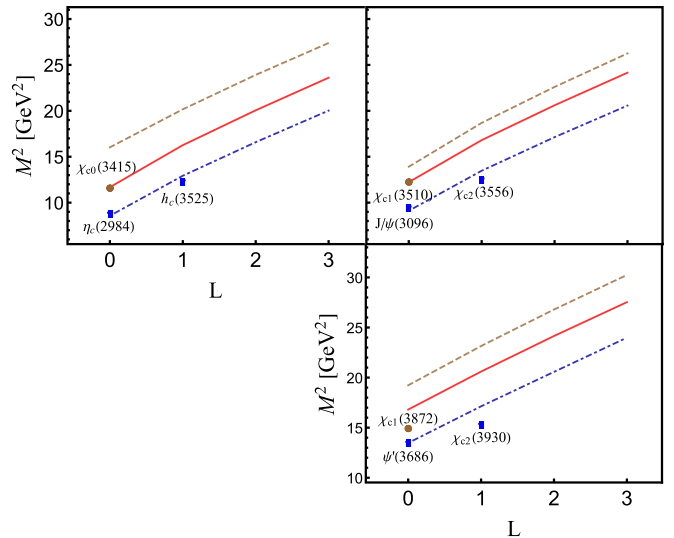


FIG. 5. Regge trajectories for the supersymmetric meson-baryon-tetraquark partners for the doubly charmed (heavy-heavy) sector. The results are compared to the PDG data [36]. The mesons, baryons, and tetraquarks trajectories are indicated by dot-dashed-blue, solid-red, and dashed-brown lines, respectively. For the left panels, $S = 0$ and for the right panels, $S = 1$.

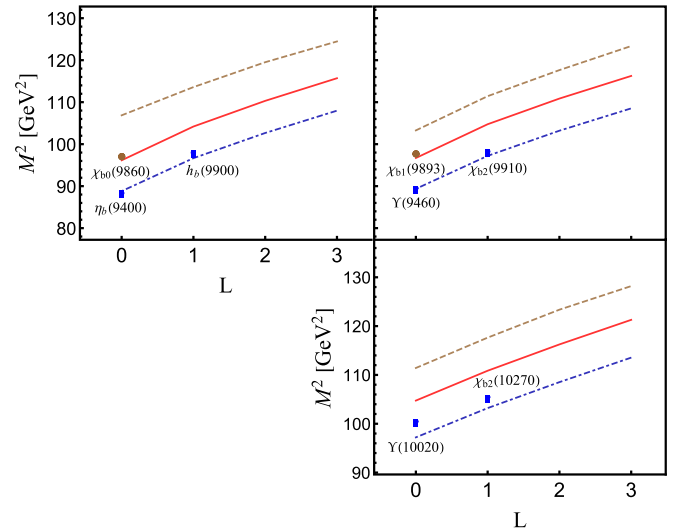


FIG. 6. Regge trajectories for the supersymmetric meson-baryon-tetraquark partners for the doubly bottom (heavy-heavy) sector. The results are compared to the PDG data [36]. The mesons, baryons, and tetraquarks trajectories are indicated by dot-dashed-blue, solid-red, and dashed-brown lines, respectively. For the left panels, $S = 0$ and for the right panels, $S = 1$.

In addition, where appropriate, the charge conjugation of mesons/tetraquarks is given by

$$C = (-1)^{n_{\parallel}+L_M+S_M} = (-1)^{n_{\parallel}+L_T+S_T-1}. \quad (41)$$

A posteriori, we find that

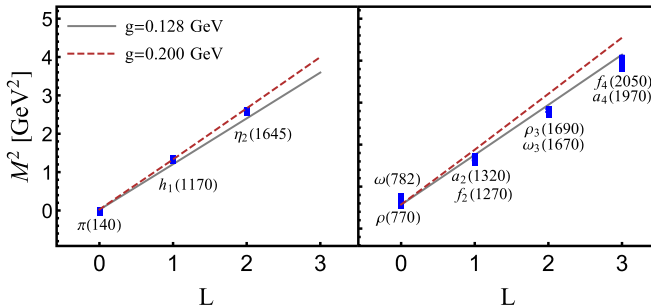


FIG. 7. Regge trajectories for π and ρ families using different values of g , e.g., $g = 0.128$ GeV (solid gray) and $g = 0.200$ GeV (dashed dark red).

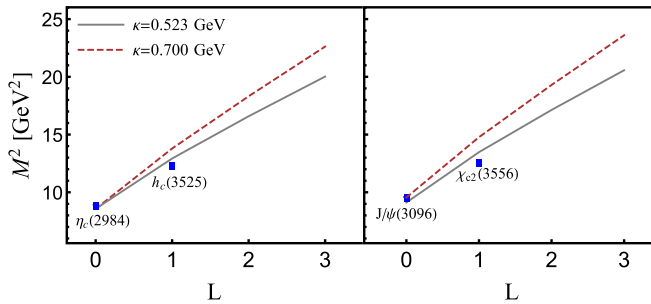


FIG. 8. Regge trajectories for η_c and J/ψ families using different values of κ , e.g., $\kappa = 0.523$ GeV (solid gray) and $\kappa = 0.700$ GeV (dashed dark red).

$$n_{\parallel} \geq n_{\perp} + L, \quad (42)$$

i.e., in any hadron, an orbital and/or radial excitation in the transverse dynamics is always accompanied by an excitation in the longitudinal dynamics. This is a signature of the underlying link between the holographic Schrödinger equation and the 't Hooft equation. This is perhaps not surprising since they both derive from the QCD Lagrangian, albeit in different dimensions and limits.

Fourth, the 't Hooft equation correctly predicts the scaling law of the decay constant of heavy-light mesons with the heavy quark mass: $f_M \propto 1/\sqrt{m_Q}$ [26]. Since the

TABLE VIII. Quark masses and the transverse confinement scale, κ , in GeV used in conjunction with the alternative longitudinal potential, Eq. (27). Note that we use $\sigma = 0.12$ GeV for all hadrons, and that the constraint, Eq. (44), is satisfied for hadrons with two heavy quarks.

Hadron	κ	$m_{u/d}$	m_s	m_c	m_b
Light	0.523	0.046	0.357
Heavy-light	1 c-quark	0.580	0.330	0.500	1.470
	1 b-quark	1.000	0.330	0.500	4.670
Heavy-heavy	2 c-quarks	0.600	1.470
	2 b-quarks	1.070	4.670

decay constant depends on the meson wave function at zero transverse separation, it follows that this remains true if the meson wave function is given by Eq. (3).

Unlike the holographic Schrödinger equation, the 't Hooft equation does not have exact analytical solutions. We shall solve it numerically using the matrix method outlined in Ref. [20], and already used in Ref. [21].

IV. COMPUTING THE HADRON SPECTRUM

We now use Eqs. (37), (38), (39), (40), and (41) to compute the hadron spectrum with the quark masses and values of g shown in Table I, together with $\kappa = 0.523$ GeV for all hadrons. In comparison to Ref. [21], we allow the light quark masses to vary between light and heavy-light hadrons, with the goal of achieving a better global description of the full hadron spectrum. We adopt the simplest assumption that the (anti)diquark mass is the sum of the (anti)quark masses, i.e., the (anti)diquark is essentially a cluster of two (anti)quarks. Note that we identify the superpartners as in Ref. [9]. Our results are shown in Table II for the light hadrons, in Table III for hadrons with one heavy quark, and in Table IV for hadrons with two heavy quarks.

In general, our meson and baryon masses are in good agreement with the data, with a discrepancy not exceeding 13%, except for $\eta'(958)$, where it is 21%. For the tetraquark candidates, the discrepancy does not exceed 18%, with notable exceptions for $f_0(500)$ and $f_0(980)(a_0(980))$, where the discrepancies are very large. The agreement for mesons and baryons is thus more impressive than for tetraquarks. In fact, the large discrepancies for the tetraquark candidates, $f_0(500)$ and $f_0(980)(a_0(980))$, are already present before any supersymmetry breaking by longitudinal dynamics. This can be seen by comparing the values of M_{\perp} to the physical masses of $f_0(500)$ and $f_0(980)(a_0(980))$ in Table II. Thus, these discrepancies are mostly inherited from the original formulation of supersymmetric light-front holography, and are not alleviated by longitudinal dynamics.

It is instructive to compare our results with those obtained using the alternative longitudinal potential given by Eq. (27). In this case, an analytical formula can be derived for the meson mass spectrum [14]:

$$M_{\parallel,M}^2 = \sigma(m_q + m_{\bar{q}})(2n_{\parallel} + 1) + \sigma^2 n_{\parallel}(n_{\parallel} + 1) + (m_q + m_{\bar{q}})^2. \quad (43)$$

Reference [17] shows that the restoration of rotational symmetry in heavy-heavy mesons implies the constraint

$$\sigma = \frac{\kappa^2}{m_Q + m_{\bar{Q}}}, \quad (44)$$

which is to be contrasted with the analogous constraint, $g = \kappa$, for the 't Hooft potential: see Eq. (35) and Eq. (36).

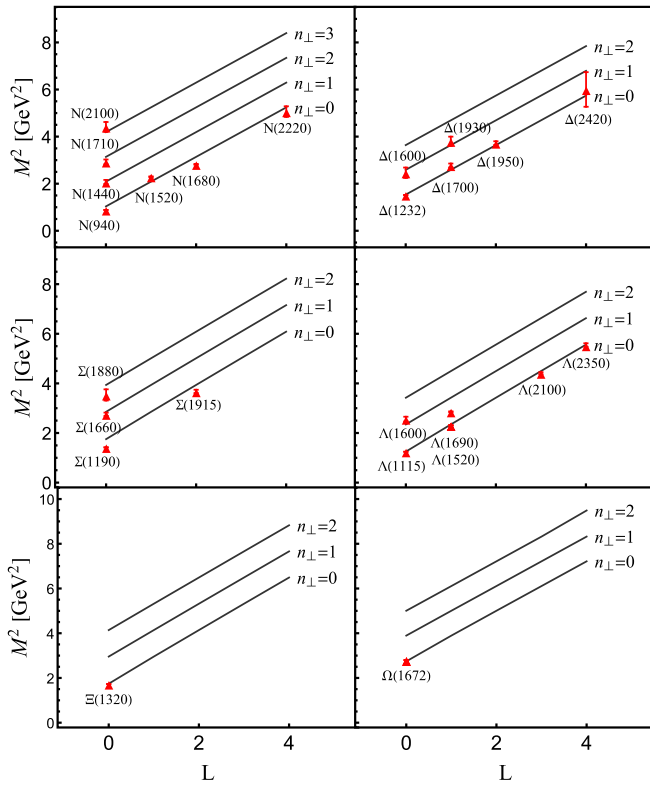


FIG. 9. Regge trajectories for the light baryons, compared to the PDG data [36].

To compute the hadron masses, we proceed in the same way as with the 't Hooft potential: within a family of superpartners, we use Eq. (43), with $\bar{q} \rightarrow [q\bar{q}]$ (for the baryon), followed by $q \rightarrow [\bar{q}\bar{q}]$ (for the tetraquark). Again, we assume that the (anti)diquark mass is twice the quark mass. This means that our goal is only to investigate the sensitivity of our results to the analytical form of the

longitudinal potential. As can be seen in Tables V, VI, and VII, the agreement with data is similar in quality to that achieved with the 't Hooft potential, provided that σ remains universal while κ is allowed to vary across the spectrum, subject to the constraint given by Eq. (44). Their numerical values, as well as those of the quark masses, are given in Table VIII.

Interestingly, it seems that either the longitudinal or the transverse confinement scale can be universal across the spectrum, depending on whether we choose Eq. (27) or the 't Hooft potential to model the longitudinal dynamics. The 't Hooft potential offers the advantage that its connection to the QCD Lagrangian is known. For this reason, it remains our focus in this paper.

We now proceed to show the Regge trajectories obtained using the 't Hooft potential: Figs. 1 and 2 for the light hadrons, Figs. 3 and 4 for hadrons with one heavy quark, and Figs. 5 and 6 for hadrons with two heavy quarks. As expected, the agreement is best for mesons and baryons. Except for the lowest-lying pseudoscalar mesons for which $M_\perp = 0$, $M_\perp \gg M_\parallel$ for light hadrons. On the other hand, $M_\parallel \gg M_\perp$ for hadrons with one or two heavy quarks. It is therefore legitimate to investigate the sensitivity of our Regge trajectories to a small variation in g (for light hadrons) or κ (for heavy hadrons), while keeping the quark masses fixed. In Fig. 7, we show the effect of changing g from 0.128 to 0.200 GeV on the π and ρ Regge trajectories. As can be seen, the slopes of the trajectories are sensitive to this variation in g . Note that, as expected, the pion mass also changes from 0.140 to 0.163 GeV but this is not visible on the mass scale of Fig. 7. Meanwhile, in Fig. 8, we illustrate the effect of changing κ from 0.523 to 0.700 GeV on the η_c and J/ψ Regge trajectories. We can see that the Regge slopes are significantly changed with this variation in κ . These observations are also typical for the other Regge

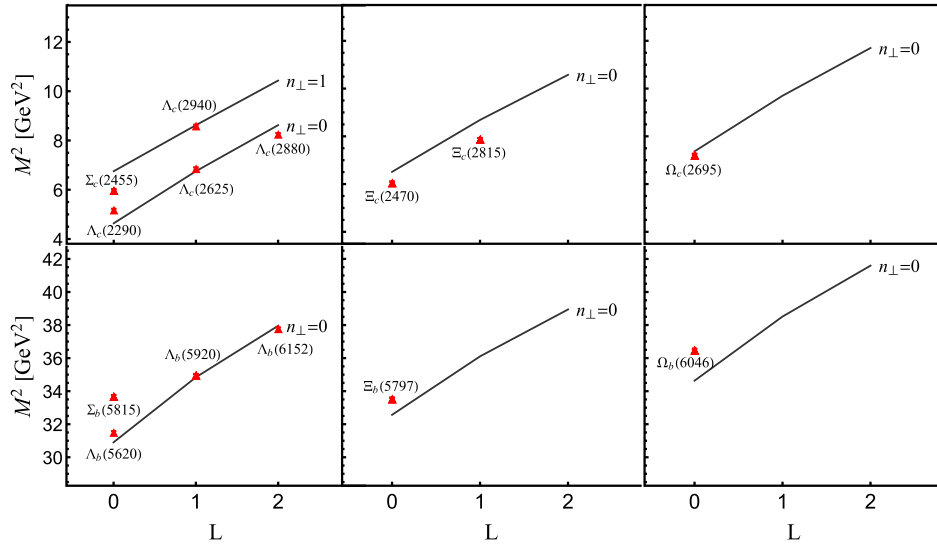


FIG. 10. Regge trajectories for the heavy baryons involving one charm (bottom) quark, compared to the PDG data [36].

trajectories. Therefore, the precise slopes and locations of Regge trajectories, for a given set of quark masses, are sensitive to both g and κ . It is worth highlighting that, in our approach, κ remains universal across the full hadron spectrum.

In Figs. 9 and 10, we compare our results for all baryons, including those with no identified superpartners from the Particle Data Group. Using $\kappa = 0.500 \pm 0.024$ GeV, we achieve very good agreement with the data.

V. CONCLUSIONS

We have shown that the 't Hooft equation is complementary to the holographic Schrödinger equation in predicting the full hadron spectrum. While the holographic Schrödinger equation generates the hadronic mass in the chiral limit of QCD with a universal emerging transverse confinement scale, the 't Hooft equation generates the contribution to the hadronic mass due to nonzero quark

masses and longitudinal confinement. Agreement with spectroscopic data spectra is generally good, while the disagreement for the tetraquark candidates, $f_0(500)$ and $f_0(980)(a_0(980))$, already present when neglecting longitudinal dynamics, persists.

ACKNOWLEDGMENTS

We thank Stan Brodsky and Guy de Téramond for useful discussions. R. S. and M. A. are supported by individual Discovery Grants No. SAPIN-2020-00051 and No. SAPIN-2021-00038) from the Natural Sciences and Engineering Research Council of Canada (NSERC). C. M. is supported by new faculty start up funding by the Institute of Modern Physics, Chinese Academy of Sciences, Grant No. E129952YR0. C. M. also thanks the Chinese Academy of Sciences President's International Fellowship Initiative for the support via Grant No. 2021PM0023.

-
- [1] S. J. Brodsky, G. F. de Teramond, H. G. Dosch, and J. Erlich, *Phys. Rep.* **584**, 1 (2015).
 - [2] S. J. Brodsky and G. F. de Teramond, *Phys. Rev. Lett.* **96**, 201601 (2006).
 - [3] G. F. de Teramond and S. J. Brodsky, *Phys. Rev. Lett.* **94**, 201601 (2005).
 - [4] G. F. de Teramond and S. J. Brodsky, *Phys. Rev. Lett.* **102**, 081601 (2009).
 - [5] S. J. Brodsky and G. F. de Teramond, *Phys. Rev. D* **77**, 056007 (2008).
 - [6] S. J. Brodsky and G. F. de Teramond, *Phys. Rev. D* **78**, 025032 (2008).
 - [7] H. G. Dosch, G. F. de Teramond, and S. J. Brodsky, *Phys. Rev. D* **92**, 074010 (2015).
 - [8] H. G. Dosch, G. F. de Teramond, and S. J. Brodsky, *Phys. Rev. D* **95**, 034016 (2017).
 - [9] M. Nielsen and S. J. Brodsky, *Phys. Rev. D* **97**, 114001 (2018).
 - [10] M. Nielsen, S. J. Brodsky, G. F. de Téramond, H. G. Dosch, F. S. Navarra, and L. Zou, *Phys. Rev. D* **98**, 034002 (2018).
 - [11] S. J. Brodsky, G. F. de Teramond, H. G. Dosch, and C. Lorce, *Int. J. Mod. Phys. A* **31**, 1630029 (2016).
 - [12] S. J. Brodsky and G. F. de Teramond, *Subnuclear series* **45**, 139 (2009).
 - [13] T. Branz, T. Gutsche, V. E. Lyubovitskij, I. Schmidt, and A. Vega, *Phys. Rev. D* **82**, 074022 (2010).
 - [14] Y. Li and J. P. Vary, [arXiv:2103.09993](#).
 - [15] M. Gell-Mann, R. J. Oakes, and B. Renner, *Phys. Rev.* **175**, 2195 (1968).
 - [16] T. Gutsche, V. E. Lyubovitskij, I. Schmidt, and A. Vega, *Phys. Rev. D* **87**, 056001 (2013).
 - [17] G. F. De Téramond and S. J. Brodsky, [arXiv:2103.10950](#).
 - [18] A. B. Scheckler and G. A. Miller, *Phys. Rev. D* **103**, 096018 (2021).
 - [19] Y. Li, P. Maris, X. Zhao, and J. P. Vary, *Phys. Lett. B* **758**, 118 (2016).
 - [20] S. S. Chabysheva and J. R. Hiller, *Ann. Phys. (Amsterdam)* **337**, 143 (2013).
 - [21] M. Ahmady, H. Dahiya, S. Kaur, C. Mondal, R. Sandapen, and N. Sharma, [arXiv:2105.01018](#).
 - [22] G. 't Hooft, *Nucl. Phys.* **B75**, 461 (1974).
 - [23] K. Hornbostel, S. J. Brodsky, and H. C. Pauli, *Phys. Rev. D* **41**, 3814 (1990).
 - [24] I. Bars and M. B. Green, *Phys. Rev. D* **17**, 537 (1978).
 - [25] A. R. Zhitnitsky, *Phys. Lett.* **165B**, 405 (1985).
 - [26] B. Grinstein and R. F. Lebed, *Phys. Rev. D* **57**, 1366 (1998).
 - [27] B. Grinstein and P. F. Mende, *Phys. Rev. Lett.* **69**, 1018 (1992).
 - [28] H. Bergknoff, *Nucl. Phys.* **B122**, 215 (1977).
 - [29] X. Ji, Y. Liu, and I. Zahed, *Phys. Rev. D* **103**, 074002 (2021).
 - [30] R. F. Lebed and N. G. Uraltsev, *Phys. Rev. D* **62**, 094011 (2000).
 - [31] B. Ma and C.-R. Ji, *Phys. Rev. D* **104**, 036004 (2021).
 - [32] H. Umeeda, *J. High Energy Phys.* 09 (2021) 066.
 - [33] E. Katz and T. Okui, *J. High Energy Phys.* 01 (2009) 013.
 - [34] G. A. Miller and S. J. Brodsky, *Phys. Rev. C* **102**, 022201 (2020).
 - [35] A. P. Trajkiński, S. D. Glazek, S. J. Brodsky, G. F. de Téramond, and H. G. Dosch, *Phys. Rev. D* **90**, 074017 (2014).
 - [36] P. Zyla *et al.* (Particle Data Group), *Prog. Theor. Exp. Phys.* **2020**, 083C01 (2020).